

# Ice Formation on Nanoparticles in a Molecular Flow Linear Quadrupole Ion Trap

Denis Duft<sup>1)</sup>, Mario Nachbar<sup>2)</sup>, Thomas Dresch<sup>2)</sup> and Thomas Leisner<sup>1)2)</sup>

<sup>1)</sup> Institute for Meteorology and Climate Research – Atmospheric Aerosol Research, Karlsruhe Institute of Technology, Germany

<sup>2)</sup> Institute for Environmental Physics, University of Heidelberg, Germany

## Introduction

Ice particles in the mesosphere of Earth's atmosphere at altitudes of 80 to 100 km (50 to 60 mi) give rise to the formation of high altitude clouds, which can be observed after sunset during polar summers at latitudes 50-70 degrees. In recent years the appearance of these Noctilucent Clouds (NLC) has been increasing and they are believed to be an indicator for the presence of water vapor in this region of the atmosphere.



Figure 1: Mesospheric ice clouds as seen from the ISS, Photo: NASA, July 13th 2012

In the upper atmosphere ice particles form predominantly by heterogeneous nucleation on nanometer size particles, which are formed by the evaporation and subsequent re-condensation of meteoric material. These meteoric smoke particles (MSP) comprise mostly Iron, Silicon and Magnesium Oxides, with typical diameters of less than 10 nm. However, much about the formation of the Noctilucent clouds remains speculative.

A better understanding of the microscopic dynamics and parameters of the condensation mechanisms on the molecular level is important for modeling of mesospheric cloud formation and large scale atmospheric processes. Further insight the nucleation process and the parametrization of ice particle growth on meteoric smoke nanoparticles results from studying these interactions in a native state, which closely simulates realistic conditions in the upper atmosphere.

We introduce a molecular flow linear quadrupole ion trap ice cell (MICE) coupled to a time-of-flight mass detector. The system is specifically designed for the investigation of supersaturated vapor condensation on the surface of nanoparticles.

## Methods

### Nanoparticle Generator

Nanoparticles were produced in a Microwave Plasma Reactor from volatile precursors like Ferrocene, Tetraethylorthosilicate (TEOS) or Magnesocene in a flow of Helium and Oxygen at 60mbar. Particle growth can be adjusted by controlling the precursor partial pressures and gas flows. Besides pure Iron Oxides ( $\text{Fe}_3\text{O}_4$ ) or Silicates ( $\text{SiO}_2$ ) it is also possible to generate mixed

$\text{Fe}_n\text{O}_x\text{Si}_m\text{O}_y$  nanoparticles. Direct Electron Microscope imaging as well as charged particle beam deflection methods has shown that nanoparticles with diameters of only a few nanometers are abundantly generated in the plasma reactor.



Figure 2: Microwave Plasma Nanoparticle Generator

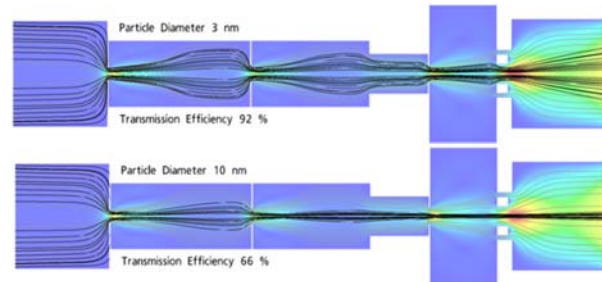


Figure 3: Aerodynamic lens focusing for two particle diameters. J. Meinen (2009)

### Aerodynamic Lens

Nanoparticles are swept from the Plasma Reactor by the constant flow of Helium (3000 sccm) at a pressure of typically 60mbar. Pressure at this stage is still too high for further analysis in a mass spectrometer requiring efficient particle transport through series of differential pumping stages. Optimal particle transport can be achieved by aerodynamic focusing, which was introduced by Liu et al., and Wang et al. For our experiment an aerodynamic lens was optimized by computer modeling for sub 10nm particles (J. Meinen et al 2009, Figure 3).

The charged nanoparticles emerging from the aerodynamic lens were characterized by electrostatic deflection and chopped beam time-of-flight analysis. Under normal operating conditions nanoparticles of all sizes emerge from the ADL with a constant velocity of (400 $\pm$ 30) m/s. Using this velocity and assuming one elementary charge, gives particle mass as a function of deflection voltage in the 90 degree quadrupole deflector DF1 (see Figure 4).

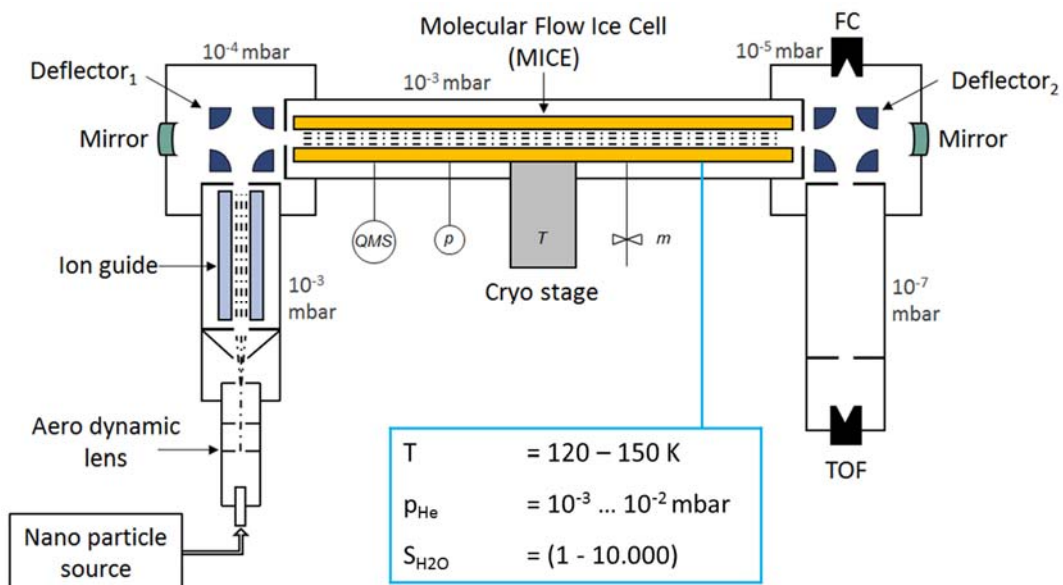


Figure 4: The MICE Experiment

## Molecular Flow Ice Cell (MICE)

At the heart of the experiment is the “Molecular Flow Ice Cell” (MICE, Figure 4). It consists of a large linear quadrupole ion trap specifically equipped as a supersaturation cell for the investigation of ice particle nucleation.

A supersaturation cell comprises in principle two walls held at different temperatures, each covered with a layer of liquid or ice. In the molecular flow supersaturation cell the temperature in the entire space enclosed by the “warm” and “cold” walls assumes essentially the mean temperature of both walls, yet the vapor concentration is constant and determined largely by the warm wall. Hence a nearly constant level of supersaturation can be achieved in the entire space.

The quadrupole ion trap of MICE consists of four copper rods (480mm) with semicircular cross section  $r = 8$  mm, mounted in a circle with  $r_0 = 7$ mm. RF only operation of the linear ion trap is achieved by means of a home built rf generator with  $U_{p-p} = 200$ - $2000$ V and a variable frequency  $f = 20$ - $100$ kHz. The typical Helium background pressure is 0.004 mbar.

In MICE the quadrupole rods act as the “cold walls” whereas special heated surfaces behind and between the rods act as the “warm walls” of the super-saturator. Computer modeling as shown in Figure 5 established suitable operating conditions for warm and cold ice covered walls to achieve the desired temperature, density and super-saturation profiles in the quadrupole cell.

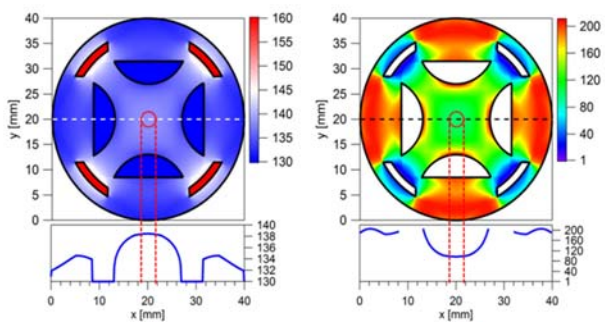


Figure 5: Profiles of Temperature [K] (left) and S values (right); the arrows indicate the extend of the ion cloud in the trap

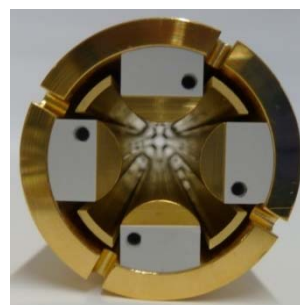


Figure 6: View of the MICE quadrupole ion tarp

Ion storage experiments have shown that the nanoparticle trap can hold up to  $10^8$  singly charged nanoparticles with negligible losses over time periods well in excess of the duration of a typical experiment. In a typical experiment,  $10^7$  size selected nanoparticles were trapped in the in the cell, where they interact with the supersaturated vapor between a few seconds and up to 1 hour.

At predetermined intervals, small fractions ( $<1\%$ ) of the particle population are extracted through the exit gate of the ion trap and injected into the linear Wiley-McLaren time-of flight mass spectrometer. The TOF is equipped with a high energy conversion dynode “Daley detector” for enhanced detection of the massive singly charged particles. Nanoparticles in the ion trap will accumulate molecules from the supersaturated vapor and grow in mass. The increase in mass is directly measured in the Time-of-Flight mass spectrometer.

## Results

Figure 7 shows the Time-of-Flight mass spectra for two different values of supersaturation  $S$ . Each trace represents a spectrum taken after different trapping duration ranging from 1.5 to 96.5 seconds. At 1.5 seconds trapping time the particles still have essentially their original mass. At  $S=4$  the particle mass quickly reaches an equilibrium. At higher  $S$  values the particles begin to grow rapidly.

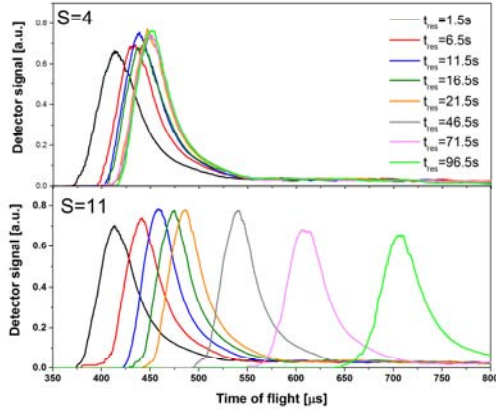


Figure 7: Time-of-Flight spectra (smoothed)

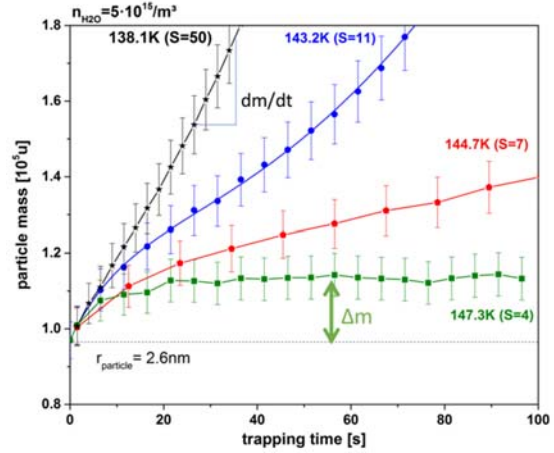


Figure 8: particle mass as a function of trapping time for different  $S$  values

Plotting particle growth as a function of trapping time for different  $S$  values (Figure 8) shows a transition from an equilibrium regime at low supersaturation to a rapid and accelerating growth regime at high values of  $S$ . The red trace indicates the transition point with critical supersaturation for nucleation of ice particles. Particle growth curves like these were recorded for different particles sizes and for Silicon Oxide ( $\text{SiO}_2$ )<sub>n</sub> and Iron Oxide ( $\text{Fe}_3\text{O}_4$ )<sub>n</sub> nanoparticles.

The energy of desorption can be directly evaluated from the equilibrium regime at low supersaturation. For this we consider the incoming flux  $J_{in}$  and the outgoing flux  $J_{out}$ . The outgoing flux is given by the Polanyi-Wigner equation with a correction factor for the Kelvin effect. At equilibrium  $J_{in} = J_{out}$ .

$$J_{in} = \frac{n_{H_2O}}{4} * v_{therm} = \frac{n_{H_2O}}{4} * \sqrt{\frac{8kT_a}{\pi m_{H_2O}}} \quad J_{out} = S_K(r) * c_s * \nu * \exp\left(\frac{-\Delta G_{des}}{kT_p}\right)$$

$n_{H_2O}$	number density of water molecules
$v_{therm}$	thermal velocity of vapor molecules
$T_a, T_p$	vapor and particle temperatures, respectively
$c_s$	surface concentration of water molecules
$\nu$	frequency factor 1E13 Hz
$k$	Boltzmann constant
$S_K(r)$	Kelvin effect correction factor for small particles
$\Delta G_{des}$	Gibbs free energy of desorption

The surface concentration  $c_s = \frac{\Delta m}{m_{H_2O}} * \frac{1}{4\pi r_p^2}$  is a direct result of the measured mass increase.

Solving for the desorption energy  $\Delta G_{des}$  gives:

$$\Delta G_{des} = kT_p * \ln \left( \frac{S_K(r)c_s \sqrt{2\pi m_{H_2O}}}{n_{H_2O} \sqrt{kT_a}} \right)$$

At high supersaturation the mass growth rate is proportional to the incoming flux times the particle surface area  $A_p(t)$  which is taken as function of time as the particle grows larger, times the mass of the water molecule. Taking the outgoing flux into account and using  $p=nkT$  yields:

$$\frac{dm}{dt} = \frac{m_{H_2O} \cdot v_{therm} \cdot A_p(t) \cdot p_{sat} \cdot (S - S_{eq}(t))}{4kT_p} \cdot \alpha$$

The “sticking coefficient“  $\alpha$  is near unity within the margin of error. In Figure 10  $S_{crit}$  indicates the onset of nucleation.

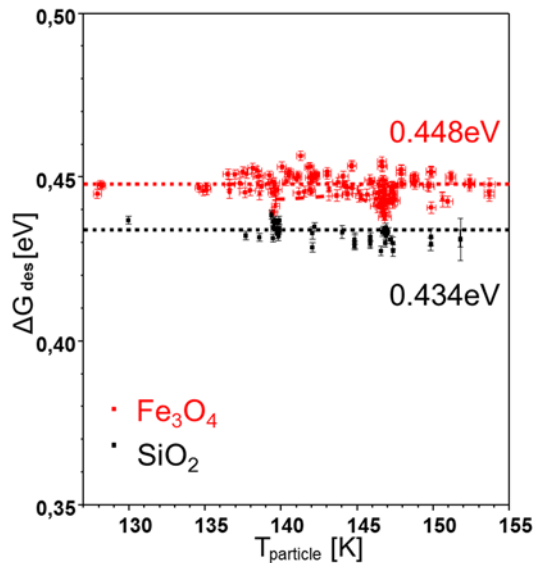


Figure 9:  $\Delta G_{des}$  for Silicon Oxide and Iron Oxide nanoparticles

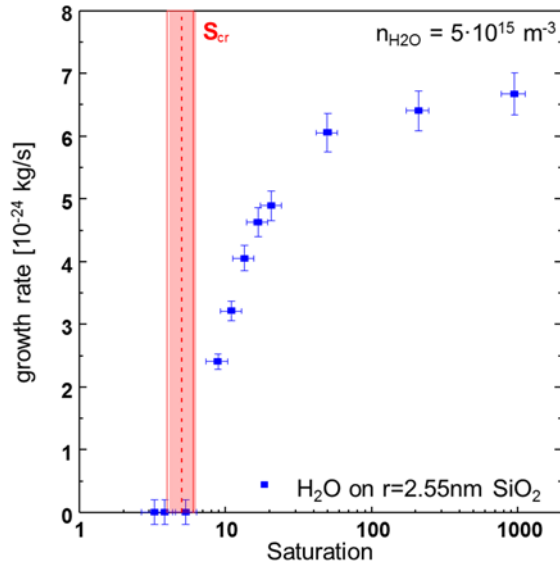


Figure 10: Critical Supersaturation for a Silica nanoparticle with diameter of 5 nm

## Conclusions

Nucleation parameters for Iron- and Silicon Oxide nanoparticles were directly measured for the first time in a laboratory experiment; as result desorption energies, sticking coefficients and critical supersaturation were determined, providing critical experimental data for the modeling of cloud formation in the upper atmosphere.

## References

Noctilucent Clouds

NASA AIM Mission Overview - *Aeronomy of Ice in the Mesosphere*

[https://www.nasa.gov/mission\\_pages/aim/overview/index.html](https://www.nasa.gov/mission_pages/aim/overview/index.html)

#### Microwave Plasma Particle Source

- Szabo, D. V., Vollath, D., Taylor, R. D., Willis, J. O., *J. Mater. Res.* 12: 2175–2182 (1997)  
Szabo, D. V., and Vollath, D., *Adv. Mater.* 11: 1313–1316 (1999)  
Baumann, W., Thekedar, B., Paur, H.–R., Seifert, H., AIChE Annual Meeting, San Francisco (2006)  
Mätzing, H., Baumann, W., Paur, H.–R., Seifert, H., *Proc. 19th Int. Symp. on Plasma Chemistry* (2009)

#### Aerodynamic Focusing

- Liu, P., Ziemann, P. J., Kittelson, D. B., McMurry, P. H., *Aerosol Sci. Technol.* 22: 293–313 (1995)  
Liu, P., Ziemann, P. J., Kittelson, D. B., McMurry, P. H., *Aerosol Sci. Technol.* 22: 314–324 (1995)  
Liu, P. S. K. et al., *Aerosol Sci. Technol.* 41: 721–733 (2007)  
Wang, X., Gidwani, A., Girshick, S. L., McMurry, P. H., *Aerosol Sci. Technol.* 39: 624–636 (2005).  
Wang, S., Zordan, C. A., Johnston, M. V., *Anal. Chem.* 78: 1750–1754 (2006)  
Wang, X., McMurry, P., *Aerosol Sci. Technol.* 40: 320–334.  
Wang, S., Johnston, M. V., *Intl. J. Mass Spec.* 258: 50–57 (2006)  
de la Mora, J. F. (1996), *Chem. Engineering Comm.* 151: 1,101–104 (1996)  
J. Fernandez de la Mora, N. Rao, P. H. McMurry, *J. Aerosol Sci.* 21, 7, 889-909 (1990)  
Meinen, J., et al., *Aerosol Sci. Technol.* 44(4):316–328 (2010)

#### Supersaturation Ion Trap Experiment (TRAPS/MICE)

- Duft, D., Nachbar, M., Eritt, M., Leisner, T., *Aerosol Sci. Technol.*, 49(4):682–690 (2015)  
Meinen, J., Khasminkaya, S., Eritt, M., Leisner, T., Antonsson, E., Langer, B., Ruehl, E., *Aerosol Sci. Technol.*, 44(4):316–328 (2010)